Polymer Chemistry

ROYAL SOCIETY
OF **CHEMISTRY**

PAPER
Mohamed Gamal Mohamed, Hung-Ju Yen,
Shiao-Wei Kuo *et al.*
Construction of fully π-conjugated, diyne-linked conjugated
microporous polymers based on tetraphenylethene and
dibenzo[*g,p*]chrysene units for energy storage

Check for updates

Construction of fully π-conjugated, diyne-linked conjugated microporous polymers based on tetraphenylethene and dibenzo[g,p]chrysene units for energy storage†

Mohamed Gamal Mohamed, [iD] *‡[a,b] Santosh U. Sharma,‡[c] Pei-Tzu Wang,[a] Mervat Ibrahim,[d] Meng-Hao Lin,[e] Cheng-Liang Liu, [iD] [e] Mohsin Ejaz, [iD] [a] Hung-Ju Yen [iD] *[c] and Shiao-Wei Kuo [iD] *[a,f]

In recent years, the quest for efficient and durable electrode materials for supercapacitors has driven the development of novel conjugated microporous polymers (CMPs). This study presents the synthesis and comprehensive characterization of two novel π-conjugated diyne-linked CMPs, TPE-Diyne CMP and TBN-Diyne CMP, designed as electrode materials for supercapacitors. These Diyne-CMPs were synthesized *via* a palladium-catalyzed alkyne–alkyne coupling reaction in high yields. Spectroscopic analyses, including FTIR and NMR, confirmed the distinct chemical structures of TPE-Diyne and TBN-Diyne CMPs, highlighting the presence of aromatic and alkyne groups essential for their electrochemical properties. Thermogravimetric analysis (TGA) demonstrated their remarkable thermal stability up to 800 °C under N_2. Furthermore, nitrogen adsorption–desorption measurements revealed high specific surface areas of 428 m^2 g^{-1} for the TPE-Diyne CMP and 256 m^2 g^{-1} for the TBN-Diyne CMP, with well-defined microporosity. Electrochemical performance tests showed that the TPE-Diyne CMP achieved a specific capacitance of 39 F g^{-1}, a capacitance retention of 98% after 2000 charge-discharge cycles and an energy density of 3.82 Wh kg^{-1}, indicating exceptional stability and energy storage capability. Meanwhile, the TBN-Diyne CMP exhibited a specific capacitance of 32.4 F g^{-1}, a cycling stability of 92% and an energy density of 3 Wh kg^{-1}. These results underscore the significance of TPE-Diyne and TBN-Diyne CMPs as innovative and highly effective electrode materials for next-generation supercapacitors, offering enhanced performance and stability. The findings contribute valuable insights into developing advanced materials for energy storage applications, addressing the growing demand for high-performance supercapacitors in various technological fields.

Introduction

Due to rising energy demands and the imperative to shift towards sustainable energy sources,[1–10] supercapacitors have emerged as promising contenders among various energy storage technologies due to their rapid energy storage and discharge capabilities, complementing traditional batteries and capacitors.[10–15] They boast high power density, swift charging and discharging rates, and prolonged cycle life, rendering them appealing for diverse applications spanning from portable electronics and electric vehicles to renewable energy systems.[16–20] The performance of supercapacitors hinges significantly on the selection of electrode materials, which act as pivotal components for energy storage. There has been a notable increase in interest in investigating novel materials with improved electrochemical properties to advance supercapacitor technology. Various materials have undergone thorough exploration

aDepartment of Materials and Optoelectronic Science, College of Semiconductor and Advanced Technology Research, Center for Functional Polymers and Supramolecular Materials, National Sun Yat-Sen University, Kaohsiung 804, Taiwan. E-mail: mgamal.eldin12@yahoo.com, kuosw@faculty.nsysu.edu.tw
bChemistry Department, Faculty of Science, Assiut University, Assiut 71516, Egypt
cInstitute of Chemistry, Academia Sinica, Taipei 115, Taiwan. E-mail: hjyen@gate.sinica.edu.tw
dChemistry Department, Faculty of Science, New Valley University, El-Kharja, 72511, Egypt
eDepartment of Materials Science and Engineering, National Taiwan University, Taipei 10617, Taiwan
fDepartment of Medicinal and Applied Chemistry, Kaohsiung Medical University, Kaohsiung 807, Taiwan
†Electronic supplementary information (ESI) available. See DOI: https://doi.org/10.1039/d4py00421c
‡These authors contributed equally.

for electrode construction in supercapacitors, encompassing carbon-based materials,[21–23] metal oxides,[24–26] conductive polymers,[27–29] and their composites. Conductive polymers have garnered significant attention due to their unique conjugated architectures, exceptional electrical conductivity, mechanical flexibility, and adjustable physical properties.[30–34] Nonetheless, conventional conductive polymers often suffer from challenges such as low specific surface areas and significant pore dispersion. To address these limitations, researchers are developing new porous conductive polymers aimed at surpassing these constraints and maximizing capacitance performance. For instance, studies have shown that optimizing the porosity and surface area of conductive polymers can significantly improve their electrochemical performance. Thus, enhancing the physicochemical properties of the active material, particularly by augmenting the specific surface area for improved electrolyte contact and increasing the conductivity to facilitate efficient electron/ion diffusion from the electrolyte to the current collector, can elevate the specific capacity.

By incorporating carbon-based materials or templating methods to enhance the surface area and control pore size distribution, researchers have achieved substantial improvements in specific capacitance and cycling stability.[35,36] Conjugated microporous polymers (CMPs) have emerged as a promising class of materials for supercapacitor applications, owing to their distinctive blend of properties. CMPs exhibit a three-dimensional network structure composed of interconnected pores at the molecular level.[37–44] Within this category, π-conjugated microporous polymers stand out for their extensive π-conjugated system and intrinsic nanopores.[45–52] These materials boast high surface areas, rendering them well-suited for gas adsorption. Moreover, they have evolved into a novel platform for diverse applications, including nanoreactors and heterogeneous catalysts, through the integration of catalytic sites within their framework.[53–60] The extensive π-conjugated system inherent in CMPs also confers remarkable light-emitting properties, enabling the development of light-harvesting structures that effectively channel energy from the framework to encapsulated acceptors. From a synthetic standpoint, CMPs provide a unique advantage by allowing precise control over both their skeletal structures and pore architectures. This level of control facilitates the customization of CMP properties for diverse applications, rendering them highly versatile and promising materials in the realms of materials science and nanotechnology. Synthesized through the polymerization of molecular building blocks, CMPs yield highly porous materials with significant surface areas.[47,55] The conjugated backbone of CMPs imbues them with π-conjugation, thereby facilitating efficient charge transport within the material.[47] Moreover, the tunable pore size and surface chemistry of CMPs present opportunities for tailoring their electrochemical properties to meet specific application requirements.[47,55] Due to its exceptional semiconductor characteristics, graphdiyne, a type of 2D material with multiple –C≡C– couplings, has already shown significant potential in various fields such as energy conversion and storage, batteries, solar devices, and catalysis.[61–63]

Cooper *et al.* achieved the efficient synthesis of diyne-linked CMPs using Pd as a catalyst in 2008.[64] The rapid dynamic control and impact of the monomer structure led to the formation of CMPs with completely amorphous structures.[47,65–67]

This study focuses on synthesizing and characterizing a novel class of CMPs, namely, TPE-Diyne and TBN-Diyne CMPs, designed specifically as electrode materials for supercapacitors. These CMPs are engineered to possess two distinct porous networks, each tailored to optimize specific electrochemical properties relevant to supercapacitor performance. The synthesis method involves carefully controlled self-polymerization of monomeric precursors under optimized conditions to achieve the desired morphology and pore structure. Comprehensive chemical and physical analyses are conducted to systematically characterize the synthesized CMPs. Subsequently, these CMPs are evaluated as electrode materials for supercapacitors using a range of electrochemical characterization techniques, including CV, GCD, and EIS. These techniques offer valuable insights into the conduct and functionality of electrochemical CMP electrodes, facilitating a thorough understanding of their suitability for energy storage applications. This research aims to contribute to advancing supercapacitor technology by exploring innovative electrode materials with enhanced performance and sustainability.

Experimental section

Materials

Dimethylformamide (DMF, 99.8%), triethylamine (Et$_3$N, 99.5%), and palladium tetrakis(triphenylphosphine) [Pd(PPh$_3$)$_4$, 99%] were procured from Sigma-Aldrich. Triphenylphosphine (PPh$_3$, 99%) was acquired from Acros Organics. Copper(I) iodide (CuI, ≥99.5%) was obtained from Alfa Aesar. TPE-TMS and TBN-TMS were synthesized according to our previous work.[68–71]

Synthesis of TPE-TB

A mixture of K$_2$CO$_3$ (2.0 g, 14.48 mmol) and TPE-TMS (0.97 g, 1.44 mmol) in 25 mL of methanol was agitated overnight at RT under N$_2$. A pale-yellow precipitate (0.82 g, Scheme S1†) was obtained after filtration and drying. FTIR (Fig. S1†): 3273, 3042, 2109 (C≡C unit). ^{1}H NMR (Fig. S2†): 7.24–6.93 (8H), 3.06 (≡C–H). ^{13}C NMR (Fig. S3†): 144–121.3, 83.86 and 78.19 (≡C–H).

Synthesis of TBN-TB

A mixture of K$_2$CO$_3$ (5.0 g, 36.17 mmol) and TBN-TMS (4.17 g, 5.83 mmol) in methanol/DCM (250 mL : 170 mL) was agitated overnight at RT under N$_2$. Upon filtration, extraction, and drying, TBN-TB was obtained as an orange solid [3.34 g, Scheme S2†]. FTIR (Fig. S4†): 2106 (C≡C unit). ^{1}H NMR (Fig. S5†): 3.30 (s, 4H), 8.81–7.73 (12 H). ^{13}C NMR (Fig. S6†): 135.70–78.87 ppm.

Synthesis of the TPE-Diyne CMP

0.21 g of the TPE-TB monomer, 0.009 g of CuI, 0.013 g of PPh$_3$, and 0.057 g of Pd(PPh$_3$)$_4$ were combined in a 50 mL flask.

Subsequently, 15 mL each of DMF and Et$_3$N were added as reaction solvents. Afterwards, the reaction mixture was stirred and heated for 72 h at 110 °C under N$_2$. Upon completion, the resulting yellow product was subjected to Soxhlet extraction using THF and MeOH, respectively, to remove unreacted monomers and the Pd catalyst and then dried in an oven at 70 °C.

Synthesis of the TBN-Diyne CMP

0.2 g of the TBN-TB monomer, 0.07 g of CuI, 0.07 g of PPh$_3$, and 0.05 g of Pd(PPh$_3$)$_4$ were combined in a 50 mL flask. Subsequently, 15 mL each of DMF and Et$_3$N were added as reaction solvents. Afterwards, the reaction mixture was stirred and heated for 72 h at 110 °C under N$_2$. Upon completion, the resulting dark yellow product was subjected to Soxhlet extraction using THF and MeOH, respectively, to remove unreacted monomers and the Pd catalyst and then dried in an oven at 70 °C.

Results and discussion

Synthesis and characterization of TPE-Diyne and TBN-Diyne CMPs

The synthesis of TPE-TB and TBN-TB monomers involved the hydrolysis of their respective TPE-TMS and TBN-TMS monomers in the presence of K$_2$CO$_3$ in methanol at room temperature for 24 h, as depicted in Schemes S1 and S2.† The new diyne-linked CMPs, TPE-Diyne and TBN-Diyne, were synthesized under solvothermal conditions. This involved the condensation of ethynyl-TPE and ethynyl-TBN monomers in the presence of Pd(PPh$_3$)$_4$/CuI/PPh$_3$ catalysts, utilizing DMF/Et$_3$N as a mixed solvent over a period of 3 days (Fig. 1(a) and (b)). The synthesis yielded a yellow powder for the TPE-Diyne CMP and a dark yellow solid for the TBN-Diyne CMP, respectively, with a yield of approximately 97%. Spectroscopic analyses, including solid-state ^{13}C NMR spectroscopy and FTIR, were conducted to confirm the distinctive chemical compositions of TPE-Diyne and TBN-Diyne CMPs [Fig. 2(a)]. In the FTIR spectra (Fig. 2(b)), notable peaks were seen at 1600 and 1491 cm^{-1}, corresponding to the C=C stretching in phenyl rings, 2205 to 2217 cm^{-1} for the –C≡C– unit, and 3033 cm^{-1} for the stretching of aromatic C–H units. In addition, the alkynyl C–H stretching vibration peaks at approximately 3118 cm^{-1} in the FT-IR spectra of TPE-Diyne and TBN-Diyne CMPs [Fig. 2(a)] are notably weaker than those of TPE-TB and TBN-TB monomers [Fig. S1 and S4†]. The results unequivocally demonstrated the formation of fully π-conjugated diyne-linked
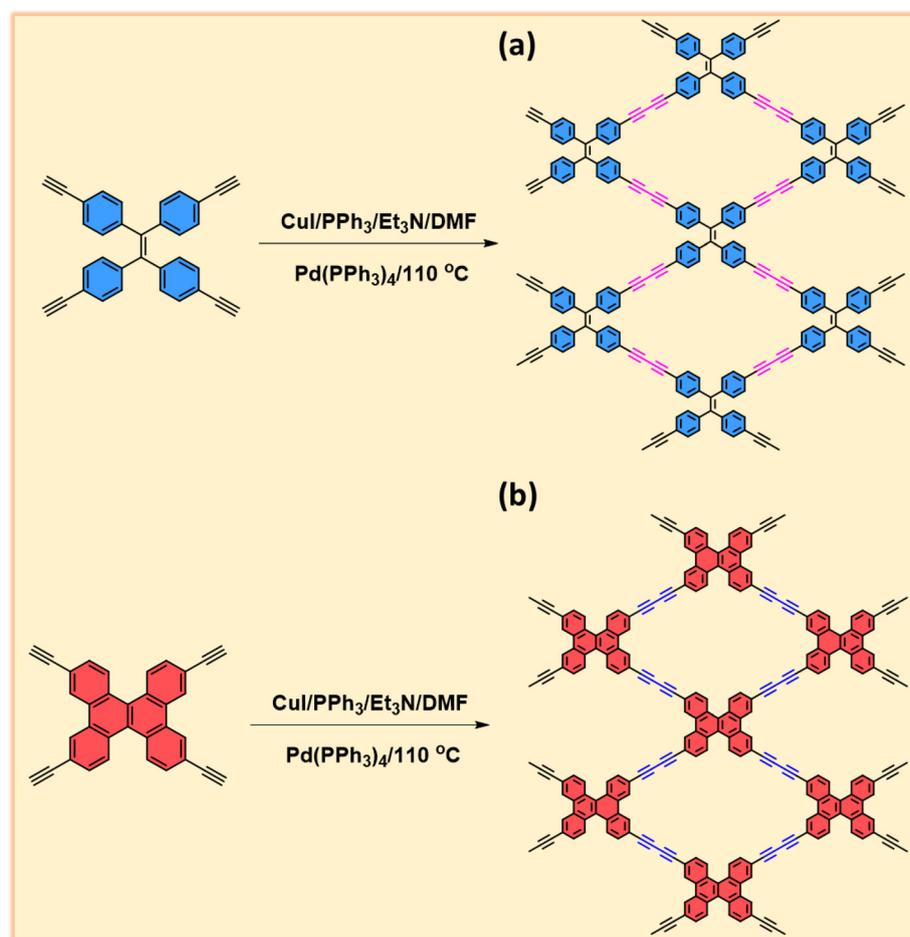

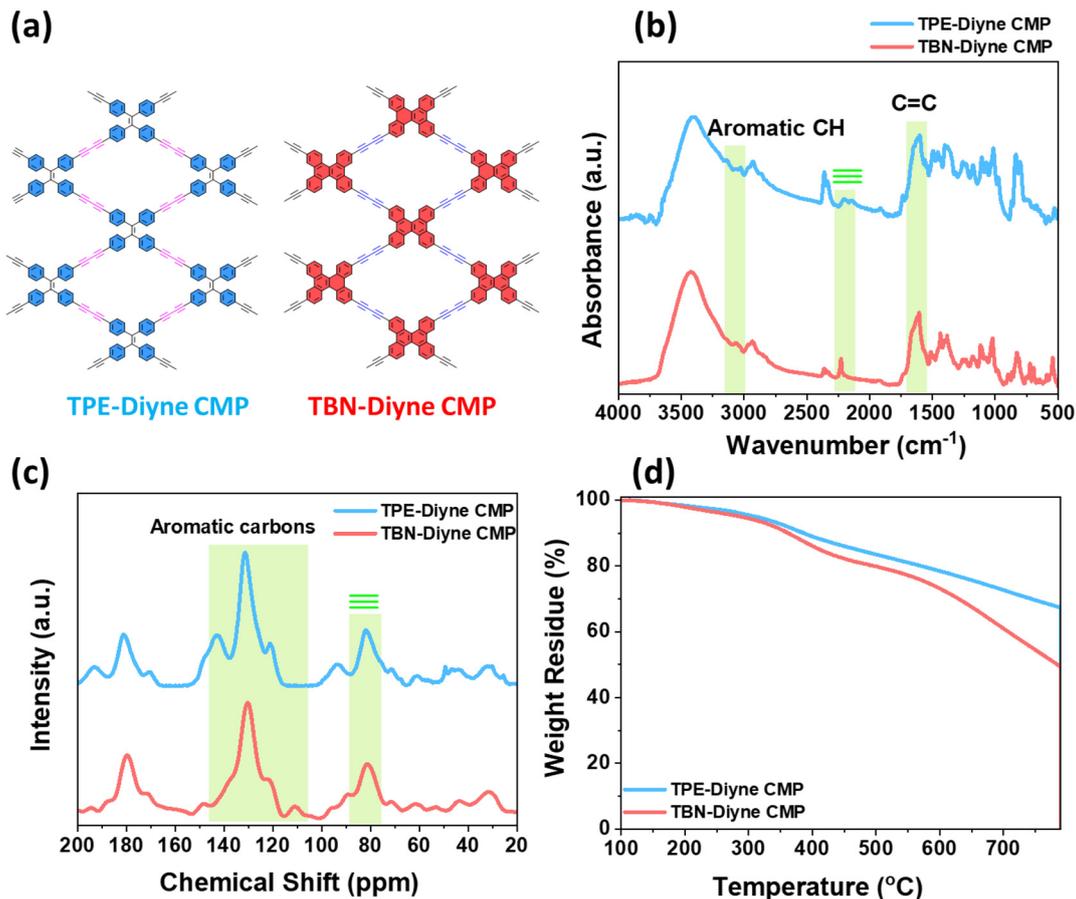**Fig. 1** Schematic method for the synthesis of the (a) TPE-Diyne CMP and (b) TBN-Diyne CMP.

Fig. 2 (a) Molecular structures, (b) FTIR, (c) solid-state ^{13}C NMR, and (d) TGA profiles of TPE–Diyne and TBN–Diyne CMPs.

CMPs. These characteristic spectral features validated the existence of alkyne (C≡C) and aromatic groups in the Diyne-CMPs frameworks. Further characterization through solid-state ^{13}C NMR spectroscopy revealed distinct signals at 142.86 and 131.48–120.82 ppm for C≡C and aromatic carbons for the TPE-Diyne CMP and 130.35–121.96 ppm for aromatic carbons for the TBN-Diyne CMP [Fig. 2(c), S7 and S8†]. The signal at *ca.* 80 ppm for C≡C groups[72] was observed in both TPE-Diyne and TBN-Diyne CMPs, as illustrated in Fig. 2(c), S7 and S8.† Additionally, their thermogravimetric analysis (TGA) depicted in Fig. 2(d) showcased the remarkable stability of both CMPs under N$_2$ up to 800 °C, with 10% weight losses occurring at 386 °C and 360 °C with char yields of around 68 and 50 wt% for TPE-Diyne and TBN-Diyne CMPs, respectively. Furthermore, the absence of crystalline diffraction peaks, as observed in Fig. S9 and S10,† suggested that the TPE-Diyne and TBN-Diyne CMPs are amorphous, according to X-ray diffraction patterns (XRD). N$_2$ sorption measurements at 77 K assessed the permanent porosity of TPE-Diyne and TBN-Diyne CMPs. The rapid N$_2$ adsorption observed at low pressure for both TPE-Diyne and TBN-Diyne CMPs, as shown in Fig. 3(a) and (b), indicates that these samples have a microporous structure. The TPE-Diyne CMP exhibits typical type IV and type I isotherms, suggesting the presence of both microporous and mesoporous structures within its framework. In contrast, the TBN-Diyne CMP displays a type I isotherm, indicating a microporous structure, as illustrated in Fig. 3(a) and (b). The typical type IV and I isotherms exhibited by TPE-Diyne and TBN-Diyne CMPs [Fig. 3(a) and (b)], respectively, suggest the presence of microporous and mesoporous structures within their frameworks. Analysis of the adsorption curves revealed Brunauer–Emmett–Teller (BET) specific surface areas of 428 and 256 m^2 g^{-1} for TPE-Diyne and TBN-Diyne CMPs, respectively. Moreover, the total pore volumes (V_{total}) of TPE-Diyne and TBN-Diyne CMPs were determined to be 0.24 and 0.31 cm^{-3} g^{-1}, respectively, based on N$_2$ adsorption measurements. Furthermore, the pore size distribution (PSD) study conducted using the NLDFT model unveiled the presence of distinct micropores and mesopores, with average sizes of 1.66 and 2.95 nm for the TPE-Diyne CMP and 1.80, 2.19, and 2.77 nm for the TBN-Diyne CMP, respectively [Fig. 3(c) and (d)]. SEM images revealed irregularly shaped nanorods with aggregated spherical particles for the TPE-Diyne CMP [Fig. S11(a and b)†] and irregularly aggregated spheres for the TBN-Diyne CMP [Fig. S11(c and d)†]. Additionally, SEM-EDS data [Fig. S11(e–h)†] confirmed the presence of aromatic carbons (C atoms) within both CMP frameworks. The porous structure and lack of long-range order in both CMPs were verified by TEM pictures [Fig. S11(i–l)†].
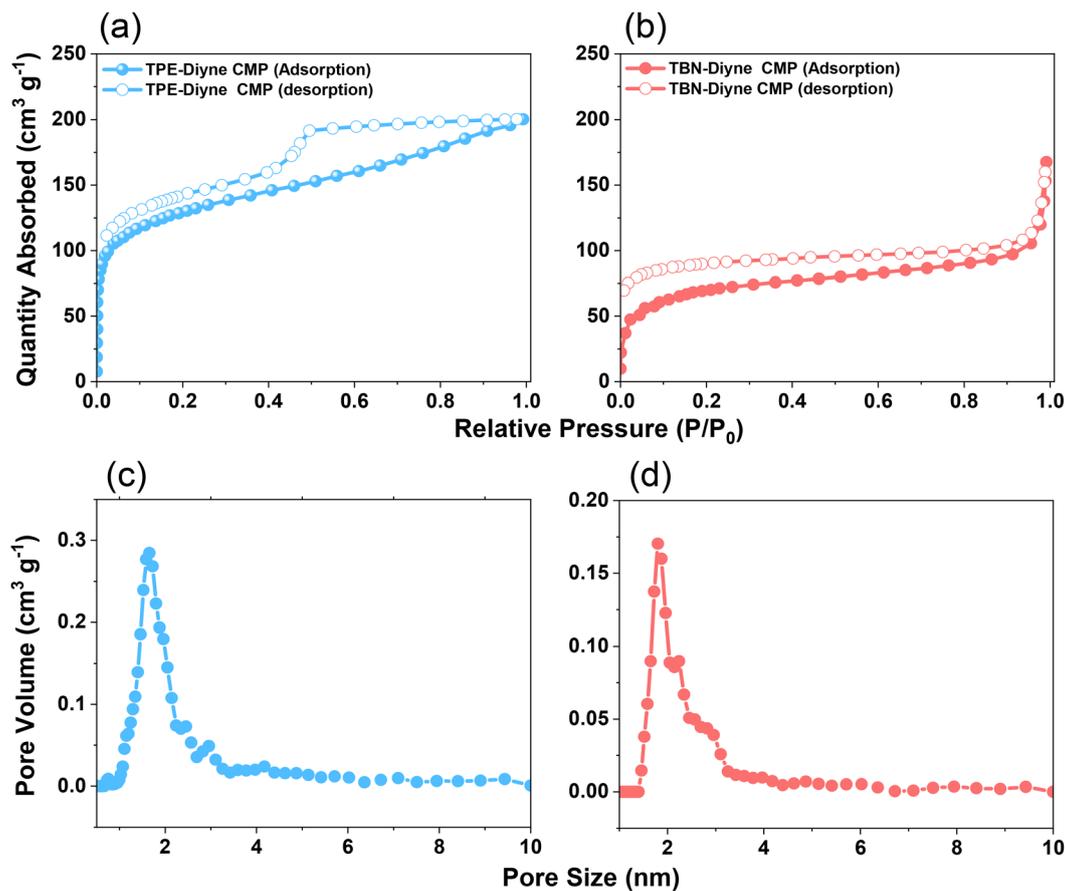
Fig. 3 (a and b) N₂ sorption isotherms and (c and d) PSD profiles of the TPE–Diyne CMP (a and c) and TBN–Diyne CMP (b and d).

Electrochemical performance of TPE-Diyne and TBN-Diyne CMPs

The electrochemical performance of TPE-Diyne and TBN-Diyne CMPs were evaluated using CV and GCD techniques in a three-electrode setup. The aqueous solution containing 1.0 M KOH served as the electrolyte. The reference, counter, and working electrodes were Hg/HgO, platinum, and glassy carbon, respectively. CV curves for TPE-Diyne and TBN-Diyne CMPs are depicted in Fig. 4(a) and (b), respectively, covering a potential range of −1.0 to 0.0 V (*vs.* Hg/HgO) at varying scan rates from 5 to 200 mV s⁻¹. Both CMPs exhibited CV curves with a characteristic rectangular-like humped shape that remained consistent across scan rates, indicating stability during the current sweep and capacitive behavior typical of electric double-layer capacitors (EDLCs).[73–77] The emergence of redox peaks in the cyclic voltammetry analysis of these fully π-conjugated, diyne-linked CMPs can be attributed to their unique structural characteristics. TPE-Diyne and TBN-Diyne CMPs possess a π-conjugated structure, enabling the delocalization of π-electrons along the polymer backbone. Moreover, the presence of electron-rich phenyl groups within the CMPs facilitates the donation of electrons during redox processes, leading to the formation of radical species. These radical species contribute to the observed redox peaks in the cyclic

voltammetry curves. Additionally, TPE-Diyne and TBN-Diyne CMPs often exhibit pseudocapacitive behavior arising from faradaic redox reactions occurring at the surface or within the pores of the material. The high surface area and well-defined microporous structure of TPE-Diyne and TBN-Diyne CMPs provide ample active sites for ion adsorption and redox reactions, thereby facilitating the appearance of redox peaks in the electrochemical profiles. Moving forward, the materials' capacitances and GCD patterns were investigated in a range of current densities from 0.5 to 20 A g⁻¹ [Fig. 4(c) and (d)]. A bowed-triangle structure was seen in all GCD curves, suggesting a mixture of EDLC and pseudocapacitive characteristics, likely attributed to the unique structural characteristics explained above. Both CMPs had longer discharging times than charging times, which may indicate increased capacitance. Notably, the TPE-Diyne CMP exhibited a longer discharging time than the TBN-Diyne CMP, indicating a higher capacitance. To accurately understand the charging harvesting mechanism, it is essential to calculate the percentages of surface-controlled capacitive and diffusion-controlled processes contributing to the total charge obtained (Q_{total}) [eqn (1)]. In accordance with the Trasatti approach,[78,79] in this scenario, following the application of the potential sweep rate to its maximum value, only the surface activities took place, and the
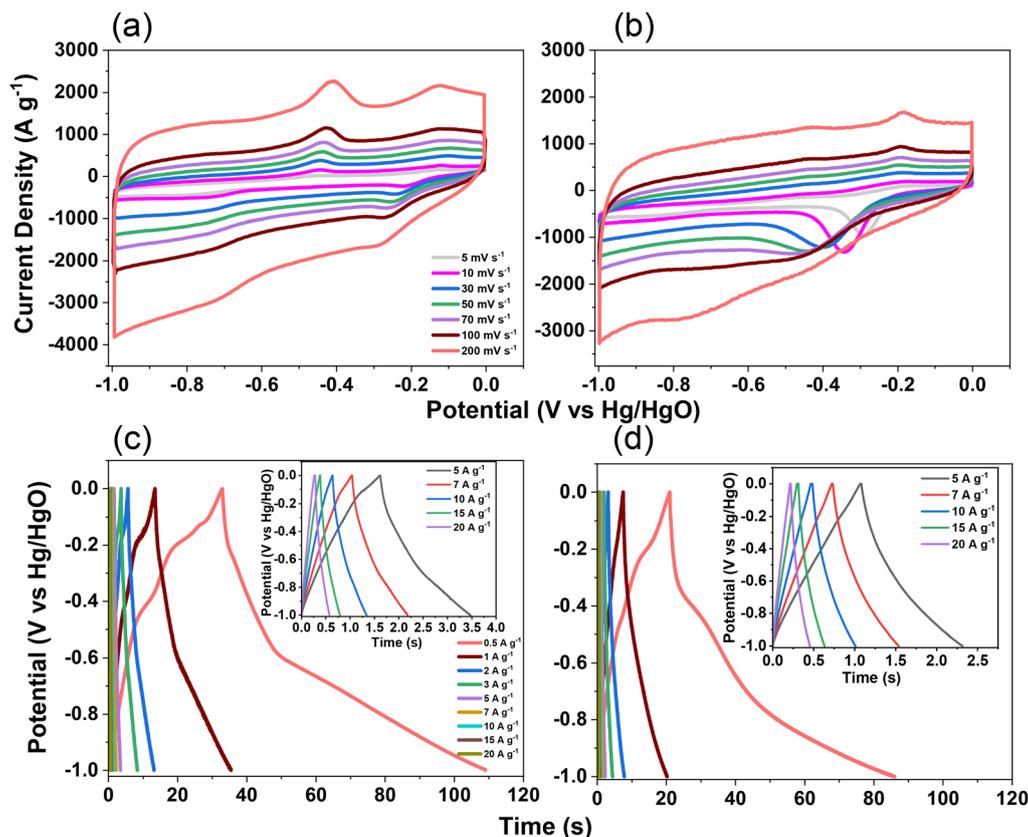
Fig. 4 (a and b) CV curves and (c and d) GCD curves of the (a and c) TPE-Diyne CMP and (b and d) TBN-Diyne CMP.

stored charge corresponds to the outer charge (Q_{outer}), as illustrated in Fig. 5(a) and (b).

$$Q = Q_{outer} + K\nu^{0.5} \qquad (1)$$

where ν (mV s^{-1}) is the potential sweep rate, K is a constant, and Q is the capacity (C g^{-1}) derived from each CV at a comparable potential sweep rate. To obtain the value of Q_{outer}, the intercept of the Q versus $\nu^{-0.5}$ plot was used. Furthermore, a
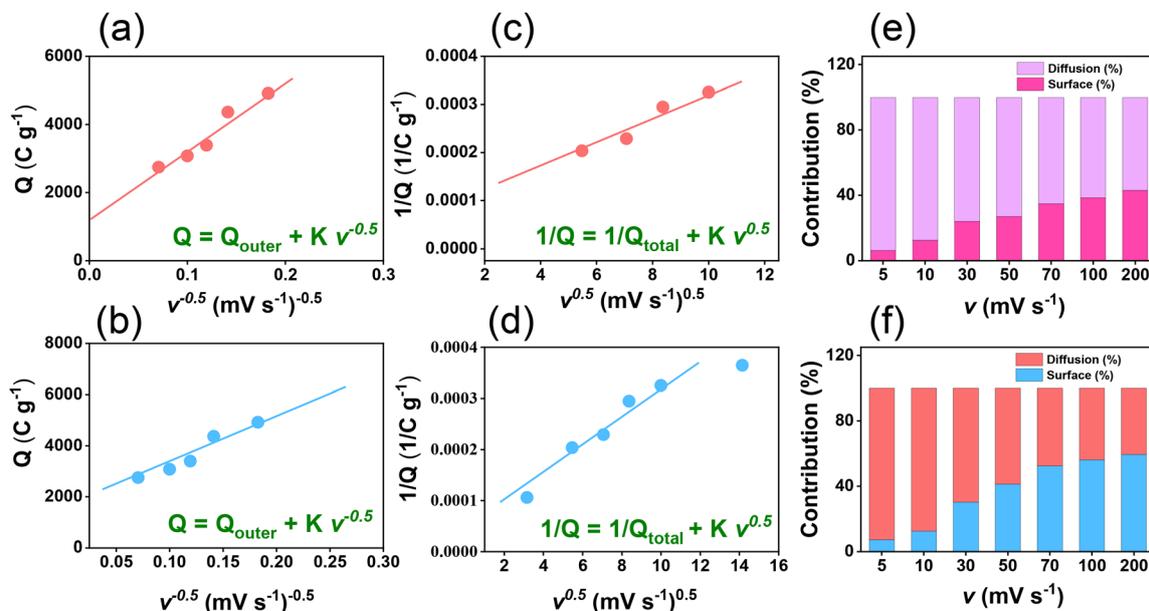

Fig. 5 (a and b) Relationship between Q (C g^{-1}) and $\nu^{-0.5}$ (mV s^{-1})$^{-0.5}$, (c and d) $1/Q$ vs. $\nu^{0.5}$ (mV s^{-1})$^{0.5}$, and (e and f) percentage of surface contribution and diffusion contribution for (a, c and e) TBN-Diyne CMP and (b, d and f) TPE-Diyne CMP electrodes.

lower scan rate allows for longer time intervals for ion diffusion. Conversely, the total charge (Q_{total}), which can be determined from the plot of ($1/Q$) *versus* $v^{0.5}$, as presented in Fig. 5(c) and (d), represents the stored charge in this scenario when the potential scan rate drops to its lowest values, allowing sufficient time for ion diffusion. This can be obtained using the following equation (2).

$$\frac{1}{Q} = \frac{1}{Q_{\text{total}}} + Kv^{0.5} \qquad (2)$$

Considering all of these factors, the electrodes for TBN-Diyne and TPE-Diyne CMPs exhibit outer charges of 1179 and 2098 C g^{-1}, respectively, and total charges of 8071 and 12 755 C g^{-1}, respectively. The surface and diffusion-controlled capacitive behaviors at different scan rates are illustrated in Fig. 5(e) and (f). The specific capacitance graphs of the TBN-Diyne and TPE-Diyne CMPs are also shown in Fig. 6(a). At a current density of 0.5 A g^{-1}, the TPE-Diyne and TBN-Diyne CMPs show capacitances of 39.0 and 32.4 F g^{-1}, respectively. Benefiting from its distinctive chemical composition and a

specific surface area of 428 m^2 g^{-1}, the TPE-Diyne CMP demonstrates superior performance compared to alternative materials. Additionally, the cycling stabilities of the TBN-Diyne and TPE-Diyne CMPs were investigated over 2000 cycles [10 A g^{-1}]. The TPE-Diyne CMP exhibited a higher capacity retention (98%) compared to the TBN-Diyne CMP (92%), indicating stability over extended cycling, even at high current densities [Fig. 6(b)]. Furthermore, both TPE-Diyne and TBN-Diyne CMPs demonstrated extraordinary energy densities of 3.82 and 3 Wh kg^{-1}, respectively [Fig. 6(c)]. In comparison with other CMPs and porous materials utilized as organic electrodes for supercapacitor applications, our TPE-Diyne and TBN-Diyne CMPs exhibited outstanding energy storage performance [Fig. 6(d)]. The EIS method was used to investigate the electric resistance provided by different electrodes during the ion diffusion process. Several Nyquist plots, featuring identical fitted circuits, are presented in Fig. 7(a), aiding in the determination of various electrode characteristics such as R_s (series resistance) and R_{ct} (charge transfer resistance). The fitting circuit diagram in Fig. 7(b) represents these features as R_s (series resistance),
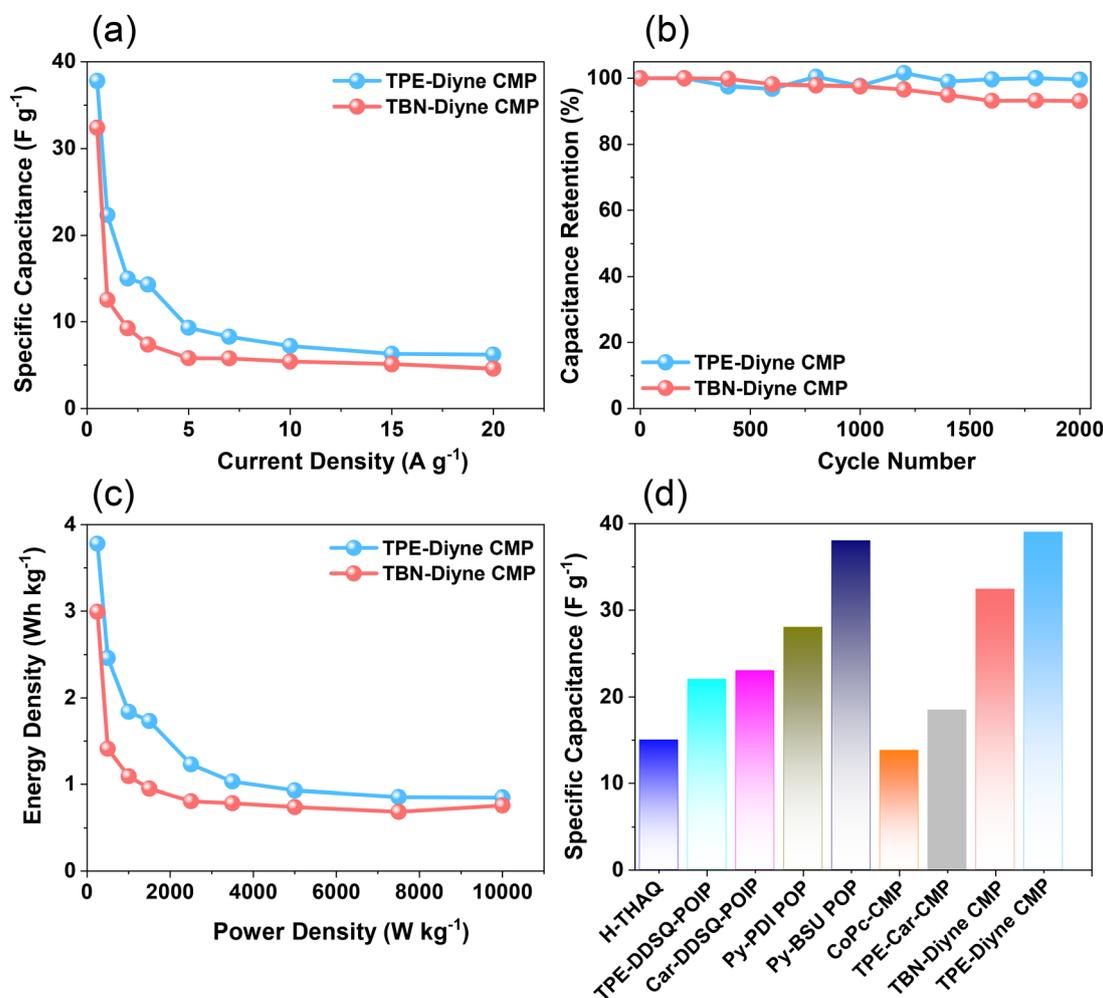

Fig. 6 (a) Specific capacitance, (b) cycling stability, (c) Ragone plot, and (d) electrochemical efficiency of TPE–Diyne and TBN–Diyne CMP electrodes with other organic precursors.
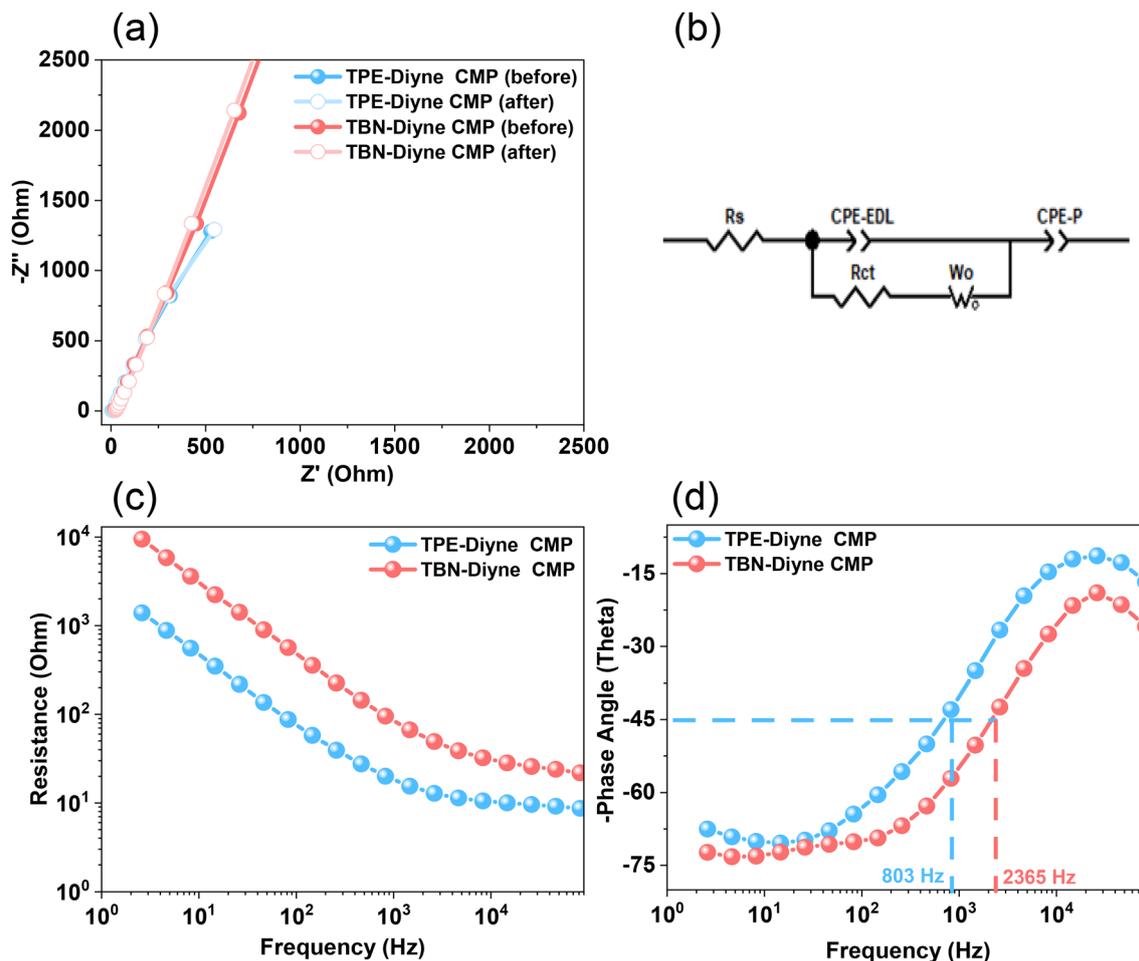
Fig. 7 (a) Nyquist plots, (b) fitted circuits, (c) Bode plots of frequency *vs.* the magnitude of resistance, and (d) Bode plots of frequency *vs.* the phase angle to determine the knee frequency of TPE–Diyne and TBN–Diyne CMPs.

R_{ct} (charge transfer resistance), CPE-EDL and CPE-P (two constant phase elements), and Z_w (Warburg element). The initial R_s values of the TPE-Diyne and TBN-Diyne CMPs electrodes were found to be 9.30 and 22.38 Ω, respectively. Despite the TPE-Diyne CMP electrode exhibiting lower R_s and R_{ct} than the TBN-Diyne CMP electrode, both displayed high specific capacities. Fig. 7(c) displays Bode plots depicting the frequency-dependent magnitude, revealing the remarkable capacitive characteristics of these electrodes. The plots feature slanted lines with negative slopes at lower frequencies, indicating their capacitive behavior while demonstrating minimum resistances at higher frequencies. Furthermore, the knee frequencies, identified at a phase angle of 45°, were determined utilizing the frequency-dependent phase angle data, as illustrated in Fig. 7(d). This observation signifies the electrodes' balanced capacitive and resistive attributes. The knee frequencies for the TPE-Diyne and TBN-Diyne CMPs were found to be 803 and 2365 Hz, respectively. In conclusion, both the TPE-Diyne and TBN-Diyne CMPs exhibited remarkable efficiency as electrode materials for energy storage applications.

DFT calculations of TPE-Diyne and TBN-Diyne CMPs

The electrical and molecular structures of CMPs determine their charge storage capacities and redox characteristics. As a result, using the Gaussian 09W software, density functional theory (DFT) computations were performed at the B3LYP/6-31G(d) level to study the link between the chemical structure and the electrochemical performance. To address the effect of long-range and non-covalent interactions, the D3BJ dispersion correction was considered. Additionally, the global minimum of each conformer in ground-state geometry was investigated by harmonic vibrational frequency to acquire the lowest energy conformer for further analysis. The molecular electrostatic potential (MESP), the lowest unoccupied molecular orbital (LUMO), and the highest occupied molecular orbital (HOMO) were computed at optimized geometries employing identical levels of theory [Fig. 8(a) and (b)]. The frontier molecular orbitals of TPE-Diyne and TBN-Diyne CMPs are shown in Fig. 8(a) and (b).

The degree of LUMO distribution dominates the electrochemical performance of both CMPs. For both TPE-Diyne and
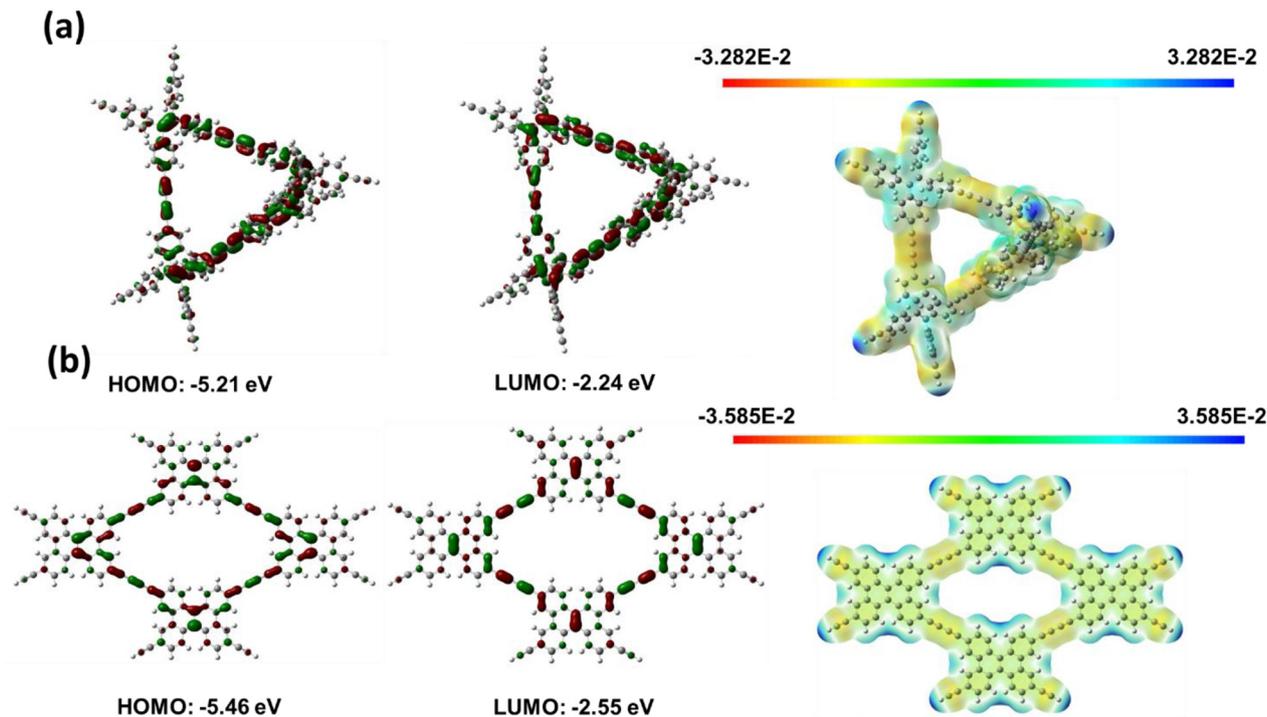
Fig. 8 DFT of (a) TPE–Diyne and (b) TBN–Diyne CMPs.

TBN-Diyne CMPs, LUMO orbitals were highly delocalized and spread over the conjugation backbones. Additionally, the energy levels of TPE-Diyne and TBN-Diyne CMPs are comparable. However, based on their molecular geometry, the molecular planarity of TPE-Diyne and TBN-Diyne CMPs is significantly different. Due to the strong steric hindrance of two benzene rings linked to the ethylene structure, the TPE-Diyne CMP would have a non-planar structure. The TBN-Diyne CMP, on the other hand, has well-defined planarity due to its fused ring topology. This variation in molecule geometry may have an additional effect on their macroscale aggregation behavior. Because of the well-defined planarity, the TBN-Diyne CMP self-aggregation would be severe owing to π–π-stacking. Therefore, the TBN-Diyne CMP would have a lower surface area compared to the TPE-Diyne CMP. A larger surface area would correspond to more active sites, resulting in improved capacitance performance in the TPE-Diyne CMP. Consequently, due to greater delocalization of molecular orbitals and a higher surface area, the TPE-Diyne CMP would achieve better electrochemical performance.

Conclusions

In summary, two robust diyne-linked CMPs derived from TPE-Diyne and TBN-Diyne were successfully synthesized using the Pd-catalyzed coupling technique for their respective monomers (TPE-TB and TBN-TB). Based on TGA data, TPE-Diyne and TBN-Diyne CMPs exhibited T_{d10} values of up to 380 and 360 °C, respectively, under a nitrogen atmosphere. Moreover, it was noted that the CMPs exhibited distinct microporosity and significant specific surface areas, with the TPE-Diyne CMP measuring 428 m^2 g^{-1} and the TBN-Diyne CMP reaching 256 m^2 g^{-1}. With a specific capacitance of 39 F g^{-1} and an impressive capacitance retention of 98% after 2000 cycles [measured at 10 A g^{-1}], the TPE-Diyne CMP demonstrates significant promise for supercapacitor applications. With full π-conjugation, a diyne structure, and a high surface area, the present study could pave the way for exploring novel approaches for constructing porous Diyne-CMPs with promising applications in energy storage or photocatalysis.

Author contributions

Mohamed Gamal Mohamed: investigation, methodology, conceptualization, supervision, and writing – original draft. Santosh U. Sharma: investigation and writing – original draft. Pei-Tzu Wang: investigation. Mervat Ibrahim: investigation. Meng-Hao Lin: investigation. Cheng-Liang Liu: investigation. Mohsin Ejaz: investigation. Hung-Ju Yen: supervision. Shiao-Wei Kuo: supervision.

Data availability

Data are contained within the article or the ESI.†

Paper

Conflicts of interest

There are no conflicts to declare.

Acknowledgements

References

1 B. P. Koirala, E. van Oost and H. van der Windt, Community energy storage: A responsible innovation towards a sustainable energy system?, *Appl. Energy*, 2018, **231**, 570–585, DOI: 10.1016/j.apenergy.2018.09.163.

2 M. Fera, R. Macchiaroli, R. Iannone, S. Miranda and S. Riemma, Economic evaluation model for the energy demand response, *Energy*, 2016, **112**, 457–468, DOI: 10.1016/j.energy.2016.06.123.

3 M. M. Samy, M. G. Mohamed, T. H. Mansoure, T. S. Meng, M. A. R. Khan, C. C. Liaw and S. W. Kuo, Solid state chemical transformations through ring-opening polymerization of ferrocene-based conjugated microporous polymers in host–guest complexes with benzoxazine-linked cyclodextrin, *J. Taiwan Inst. Chem. Eng.*, 2022, **132**, 104110, DOI: 10.1016/j.jtice.2021.10.010.

4 F. Zhao, S. Gong, H. Xu, M. Li, L. Li, J. Qi, H. Wang, Z. Wang, Y. Hu, X. Fan, C. Li and J. Liu, In Situ Constructing Amorphous V_2O_5@Ti_3C_2Tx Heterostructure for High-Performance Aqueous Zinc-Ion Batteries, *J. Power Sources*, 2022, **544**, 231883, DOI: 10.1016/j.jpowsour.2022.231883.

5 R. C. Armstrong, C. Wolfram, K. P. De Jong, R. Gross, N. S. Lewis, B. Boardman, A. J. Ragauskas, K. Ehrhardt-Martinez, G. Crabtree and M. V. Ramana, The Frontiers of Energy, *Nat. Energy*, 2016, **1**, 15020, DOI: 10.1038/nenergy.2015.20.

6 S. Chu and A. Majumdar, Opportunities and Challenges for a Sustainable Energy Future, *Nature*, 2012, **488**, 294–303, DOI: 10.1038/nature11475.

7 P. N. Singh, M. G. Mohamed, S. V. Chaganti, S. U. Sharma, M. Ejaz, J. T. Lee and S. W. Kuo, Rational Design of Ultrastable Conjugated Microporous Polymers based on Pyrene and Perylene Units as High-Performance Organic Electrode Materials for Supercapacitor Applications, *ACS Appl. Energy Mater.*, 2023, **6**, 8277–8287, DOI: 10.1021/acsaem.3c01391.

8 M. Andoni, V. Robu, D. Flynn, S. Abram, D. Geach, D. Jenkins, P. McCallum and A. Peacock, Blockchain technology in the energy sector: A systematic review of challenges and opportunities, *Renewable Sustainable Energy Rev.*, 2019, **100**, 143–174, DOI: 10.1016/j.rser.2018.10.014.

9 Y. Lv, Transitioning to Sustainable Energy: Opportunities, Challenges, and the Potential of Blockchain Technology, *Front. Energy Res.*, 2023, **11**, 1258044, DOI: 10.3389/fenrg.2023.1258044.

10 D. P. Chatterjee and A. K. Nandi, A review on the recent advances in hybrid supercapacitors, *J. Mater. Chem. A*, 2021, **9**, 15880–15918, DOI: 10.1039/D1TA02505H.

11 Z. Zhang, T. Ding, Q. Zhou, Y. Sun, M. Qu, Z. Zeng, Y. Ju, L. Li, K. Wang and F. Chi, A review of technologies and applications on versatile energy storage systems, *Renewable Sustainable Energy Rev.*, 2021, **148**, 111263, DOI: 10.1016/j.rser.2021.111263.

12 X. Zhao, B. M. Sánchez, P. J. Dobson and P. S. Grant, The role of nanomaterials in redox-based supercapacitors for next generation energy storage devices, *Nanoscale*, 2011, **3**, 839–855, DOI: 10.1039/C0NR00594K.

13 X. Wang, X. Lu, B. Liu, D. Chen, Y. Tong and G. Shen, Flexible energy–storage devices: design consideration and recent progress, *Adv. Mater.*, 2014, **26**, 4763–4782, DOI: 10.1002/adma.202205326.

14 M. G. Mohamed, M. M. Samy, T. H. Mansoure, C. J. Li, W. C. Li, J. H. Chen, K. Zhang and S. W. Kuo, Microporous Carbon and Carbon/Metal Composite Materials Derived from Bio-Benzoxazine-Linked Precursor for CO_2 Capture and Energy Storage Applications, *Int. J. Mol. Sci.*, 2022, **23**, 347, DOI: 10.3390/ijms23010347.

15 C. Zhong, Y. Deng, W. Hu, J. Qiao, L. Zhang and J. Zhang, A Review of Electrolyte Materials and Compositions for Electrochemical Supercapacitors, *Chem. Soc. Rev.*, 2015, **44**, 7484–7539, DOI: 10.1039/C5CS00303B.

16 M. G. Mohamed, H. Y. Hu, M. Madhu, M. M. Samy, I. M. A. Mekhemer, W. L. Tseng, H. H. Chou and S. W. Kuo, Ultrastable two-dimensional fluorescent conjugated microporous polymers containing pyrene and fluorene units for metal ion sensing and energy storage, *Eur. Polym. J.*, 2023, **189**, 111980, DOI: 10.1016/j.eurpolymj.2023.111980.

17 T. H. Weng, M. G. Mohamed, S. U. Sharma, S. V. Chaganti, M. M. Samy, J. T. Lee and S. W. Kuo, Ultrastable Three-Dimensional Triptycene- and Tetraphenylethene-Conjugated Microporous Polymers for Energy Storage, *ACS Appl. Energy Mater.*, 2022, **5**, 14239–14249, DOI: 10.1021/acsaem.2c02809.

18 M. G. Mohamed, M. M. Samy, T. H. Mansoure, C. J. Li, W. C. Li, J. H. Chen, K. Zhang and S. W. Kuo, Microporous Carbon and Carbon/Metal Composite Materials Derived from Bio-Benzoxazine-Linked Precursor for CO_2 Capture and Energy Storage Applications, *Int. J. Mol. Sci.*, 2022, **23**, 347, DOI: 10.3390/ijms23010347.

19 M. Ejaz, M. G. Mohamed and S. W. Kuo, Solid-state chemical transformation provides a fully benzoxazine-linked porous organic polymer displaying enhanced CO_2 capture and supercapacitor performance, *Polym. Chem.*, 2023, **14**, 249–2509, DOI: 10.1039/D3PY00158J.

20 Y. Hou, Y. Cheng, T. Hobson and J. Liu, Design and synthesis of hierarchical MnO$_2$ nanospheres/carbon nanotubes/conducting polymer ternary composite for high performance electrochemical electrodes, *Nano Lett.*, 2010, **10**, 2727–2733, DOI: **10.1021/nl101723g**.

21 M. Tong, S. Liu, X. Zhang, T. Wu, H. Zhang, G. Wang, Y. Zhang, X. Zhu and H. Zhao, Two-dimensional CoNi nanoparticles@ S, N-doped carbon composites derived from S, N-containing Co/Ni MOFs for high performance supercapacitors, *J. Mater. Chem. A*, 2017, **5**, 9873–9881, DOI: **10.1039/C7TA01008G**.

22 Z. Liu, K. Xiao, H. Guo, X. Ning, A. Hu, Q. Tang, B. Fan, Y. Zhu and X. Chen, Nitrogen-doped worm-like graphitized hierarchical porous carbon designed for enhancing area-normalized capacitance of electrical double layer supercapacitors, *Carbon*, 2017, **117**, 163–173, DOI: **10.1016/j.carbon.2017.02.087**.

23 D. Zhu, K. Cheng, Y. Wang, D. Sun, L. Gan, T. Chen, J. Jiang and M. Liu, Nitrogen-doped porous carbons with nanofiber-like structure derived from poly (aniline-co-p-phenylenediamine) for supercapacitors, *Electrochim. Acta*, 2017, **224**, 17–24, DOI: **10.1016/j.electacta.2016.12.023**.

24 Q. Ma, H. Cheng, A. G. Fane, R. Wang and H. Zhang, Recent Development of Advanced Materials with Special Wettability for Selective Oil/Water Separation, *Small*, 2016, **12**, 2186–2202, DOI: **10.1002/smll.201503685**.

25 D. Xu, W. Hu, X. N. Sun, P. Cui and X. Y. Chen, Redox additives of Na$_2$MoO$_4$ and KI: Synergistic effect and the improved capacitive performances for carbon-based supercapacitors, *J. Power Sources*, 2017, **341**, 448–456, DOI: **10.1016/j.jpowsour.2016.12.031**.

26 L. Xing, Y. Dong and X. Wu, Hierarchical Co$_3$O$_4$@Co$_9$S$_8$ nanowall structures assembled by many nanosheets for high performance asymmetric supercapacitors, *RSC Adv.*, 2018, **8**, 28172–28178, DOI: **10.1039/C8RA05722B**.

27 F. Chen, X. Liu, Z. Zhang, N. Zhang, A. Pan, S. Liang and R. Ma, Controllable fabrication of urchin-like Co$_3$O$_4$ hollow spheres for high-performance supercapacitors and lithium-ion batteries, *Dalton Trans.*, 2016, **45**, 15155–15161, DOI: **10.1039/C6DT02603F**.

28 D. P. Dubal, N. R. Chodankar, R. Holze, D. H. Kim and P. Gomez-Romero, Ultrathin mesoporous RuCo$_2$O$_4$ nanoflakes: an advanced electrode for high–performance asymmetric supercapacitors, *ChemSusChem*, 2017, **10**, 1771–1782, DOI: **10.1002/cssc.201700001**.

29 W. Li, H. Lu, N. Zhang and M. Ma, Enhancing the properties of conductive polymer hydrogels by freeze–thaw cycles for high-performance flexible supercapacitors, *ACS Appl. Mater. Interfaces*, 2017, **9**, 20142–20149, DOI: **10.1021/acsami.7b05963**.

30 Y. Ma, C. Hou, H. Zhang, M. Qiao, Y. Chen, H. Zhang, Q. Zhang and Z. Guo, Morphology-dependent electrochemical supercapacitors in multi-dimensional polyaniline nanostructures, *J. Mater. Chem. A*, 2017, **5**, 14041–14052, DOI: **10.1039/C7TA03279J**.

31 Y. Huang, H. Li, Z. Wang, M. Zhu, Z. Pei, Q. Xue, Y. Huang and C. Zhi, Nanostructured polypyrrole as a flexible electrode material of supercapacitor, *Nano Energy*, 2016, **22**, 422–438, DOI: **10.1016/j.nanoen.2016.02.047**.

32 T. Li, W. Zhu, R. Shen, H. Y. Wang, W. Chen, S. J. Hao, Y. Li, Z. G. Gu and Z. Li, Three-dimensional conductive porous organic polymers based on tetrahedral polythiophene for high-performance supercapacitors, *New J. Chem.*, 2018, **42**, 6247–6255, DOI: **10.1039/C8NJ00667A**.

33 A. Afzal, F. A. Abuilaiwi, A. Habib, M. Awais, S. B. Waje and M. A. Atieh, Polypyrrole/carbon nanotube supercapacitors: Technological advances and challenges, *J. Power Sources*, 2017, **352**, 174–186, DOI: **10.1016/j.jpowsour.2017.03.128**.

34 A. Sajedi-Moghaddam, E. Saievar-Iranizad and M. Pumera, Two-dimensional transition metal dichalcogenide/conducting polymer composites: synthesis and applications, *Nanoscale*, 2017, **9**, 8052–8065, DOI: **10.1039/C7NR02022H**.

35 L. Xie, F. Su, L. Xie, X. Guo, Z. Wang, Q. Kong, G. Sun, A. Ahmad, X. Li, Z. Yi and C. Chen, Effect of pore structure and doping species on charge storage mechanisms in porous carbon-based supercapacitors, *Mater. Chem. Front.*, 2020, **4**, 2610–2634, DOI: **10.1039/D0QM00180E**.

36 S. R. Sivakkumar, W. J. Kima, J. Ae Choi, D. R. MacFarlane, M. Forsyth and D. W. Kim, Electrochemical performance of polyaniline nanofibres and polyaniline/multi-walled carbon nanotube composite as an electrode material for aqueous redox supercapacitors, *J. Power Sources*, 2007, **171**, 1062–1068, DOI: **10.1016/j.jpowsour.2007.05.103**.

37 M. M. Samy, I. M. A. Mekhemer, M. G. Mohamed, M. H. Elsayed, K. H. Lin, Y. K. Chen, T. L. Wu, H. H. Chou and S. W. Kuo, Conjugated Microporous Polymers Incorporating Thiazolo[5,4-*d*]thiazole Moieties for Sunlight-Driven Hydrogen Production from Water, *Chem. Eng. J.*, 2022, **446**, 137158, DOI: **10.1016/j.cej.2022.137158**.

38 M. G. Mohamed, T. H. Mansoure, M. M. Samy, Y. Takashi, A. A. K. Mohammed, T. Ahamad, S. M. Alshehri, J. Kim, B. M. Matsagar, K. C. W. Wu and S. W. Kuo, Ultrastable Conjugated Microporous Polymers Containing Benzobisthiadiazole and Pyrene Building Blocks for Energy Storage Applications, *Molecules*, 2022, **27**, 2025, DOI: **10.3390/molecules27062025**.

39 A. O. Mousa, Z. I. Lin, C. H. Chuang, C. K. Chen, S. W. Kuo and M. G. Mohamed, Rational Design of Bifunctional Microporous Organic Polymers Containing Anthracene and Triphenylamine Units for Energy Storage and Biological Applications, *Int. J. Mol. Sci.*, 2023, **24**, 8966, DOI: **10.3390/ijms24108966**.

40 M. G. Mohamed, S. U. Sharma, C. H. Yang, M. M. Samy, A. A. K. Mohammed, S. V. Chaganti, J.-T. Lee and S. W. Kuo, Anthraquinone-enriched conjugated microporous polymers as organic cathode materials for high-performance lithium-ion batteries, *ACS Appl. Energy Mater.*, 2021, **4**, 14628–14639, DOI: **10.1021/acsaem.1c03270**.

41 P. N. Singh, M. G. Mohamed and S. W. Kuo, Systematic Design and Synthesis of Conjugated Microporous Polymers Containing Pyrene and Azobenzene Building Materials for

High-Performance Energy Storage, *ACS Appl. Energy Mater.*, 2023, **6**, 11342–11351, DOI: **10.1021/acsaem.3c02252**.

42 M. G. Mohamed, H. Y. Hu, S. Santhoshkumar, M. Madhu, T. H. Mansoure, C. W. Hsiao, Y. Ye, C. W. Huang, W. L. Tseng and S. W. Kuo, Design and synthesis of bifunctional conjugated microporous polymers containing tetraphenylethene and bisulfone units for energy storage and fluorescent sensing of *p*-nitrophenol, *Colloids Surf., A*, 2024, **680**, 132675, DOI: **10.1016/j.colsurfa.2023.132675**.

43 Z. Zhu, Z. Yang, Y. Fan, C. Liu, H. Sun, W. Liang and A. Li, Calcination of porphyrin-based conjugated microporous polymers nanotubes as nanoporous N-rich metal-free electrocatalysts for efficient oxygen reduction reaction, *ACS Appl. Energy Mater.*, 2020, **3**, 5260–5268, DOI: **10.1021/acsaem.0c00079**.

44 Y. Liao, Z. Cheng, M. Trunk and A. Thomas, Targeted control over the porosities and functionalities of conjugated microporous polycarbazole networks for CO_2-selective capture and H_2 storage, *Polym. Chem.*, 2017, **8**, 7240–7247, DOI: **10.1039/C7PY01439B**.

45 W. Zhang, S. Li, X. Tang, J. Tang, C. Pan and G. Yu, Phenothiazine core promoted charge transfer in conjugated microporous polymers for photocatalytic Ugi-type reaction and aerobic selenation of indoles, *Appl. Catal., B*, 2020, **272**, 118982, DOI: **10.1016/j.apcatb.2020.118982**.

46 Q. Xie, Y. Yang, W. Zhang, Z. Gao, X. Li, J. Tang, C. Pan and G. Yu, Polarization-induced charge separation in conjugated microporous polymers for efficient visible light-driven C-3 selenocyanation of indoles, *Chem. Sci.*, 2021, **12**, 5631–5637, DOI: **10.1039/D0SC06951E**.

47 J. S. M. Lee and A. I. Cooper, Advances in conjugated microporous polymers, *Chem. Rev.*, 2020, **120**, 2171–2214, DOI: **10.1021/acs.chemrev.9b00399**.

48 M. G. Mohamed, E. C. Atayde Jr, M. B. Matsagar, J. Na, Y. Yamauchi, K. C. W. Wu and S. W. Kuo, Construction Hierarchically Mesoporous/Microporous Materials Based on Block Copolymer and Covalent Organic Framework, *J. Taiwan Inst. Chem. Eng.*, 2020, **112**, 180–192, DOI: **10.1016/j.jtice.2020.06.013**.

49 Y. Ye, M. G. Mohamed, W. C. Chen and S. W. Kuo, Integrating the multiple functionalities in metalloporphyrin porous organic polymers enabling strong polysulfide anchoring and rapid electrochemical kinetics in Li–S batteries, *J. Mater. Chem. A*, 2023, **11**, 9112–9124, DOI: **10.1039/D2TA09232H**.

50 W. Lyu, W. Zhang, H. Liu, Y. Liu, H. Zuo, C. Yan, C. F. J. Faul, A. Thomas, M. Zhu and Y. Liao, Conjugated Microporous Polymer Network Grafted Carbon Nanotube Fibers with Tunable Redox Activity for Efficient Flexible Wearable Energy Storage, *Chem. Mater.*, 2020, **32**, 8276–8285, DOI: **10.1021/acs.chemmater.0c02089**.

51 J. X. Jiang, F. Su, A. Trewin, C. D. Wood, N. L. Campbell, H. Niu, C. Dickinson, A. Y. Ganin, M. J. Rosseinsky and Y. Z. Khimyak, Conjugated Microporous Poly(aryleneethynylene) Networks, *Angew. Chem., Int. Ed.*, 2007, **46**, 8574–8578, DOI: **10.1002/anie.200701595**.

52 Y. Kou, Y. Xu, Z. Guo and D. Jiang, Supercapacitive energy storage and electric power supply using an aza–fused π–conjugated microporous framework, *Angew. Chem.*, 2011, **123**, 8912–8916, DOI: **10.1002/anie.201103493**.

53 A. Thomas, P. Kuhn, J. Weber, M. M. Titirici and M. Antonietti, Porous polymers: enabling solutions for energy applications, *Macromol. Rapid Commun.*, 2009, **30**, 221–236, DOI: **10.1002/marc.200800642**.

54 J. X. Jiang, C. Wang, A. Laybourn, T. Hasell, R. Clowes, Y. Z. Khimyak, J. Xiao, S. J. Higgins, D. J. Adams and A. I. Cooper, Metal–organic conjugated microporous polymers, *Angew. Chem.*, 2011, **123**, 1104–1107, DOI: **10.1002/anie.201005864**.

55 M. G. Mohamed, A. F. M. El-Mahdy, M. G. Kotp and S. W. Kuo, Advances in Porous Organic Polymers: Syntheses, Structures, and Diverse Applications, *Adv. Mater.*, 2022, **3**, 707–733, DOI: **10.1039/D1MA00771H**.

56 M. M. Samy, M. G. Mohamed, S. U. Sharma, S. V. Chaganti, J. T. Lee and S. W. Kuo, An Ultrastable Tetrabenzonaphthalene-Linked conjugated microporous polymer functioning as a high-performance electrode for supercapacitors, *J. Taiwan Inst. Chem. Eng.*, 2024, **158**, 104750, DOI: **10.1016/j.jtice.2023.104750**.

57 R. S. Sprick, Y. Bai, A. A. Y. Guilbert, M. Zbiri, C. M. Aitchison, L. Wilbraham, Y. Yan, D. J. Woods, M. A. Zwijnenburg and A. I. Cooper, Photocatalytic Hydrogen Evolution from Water Using Fluorene and Dibenzothiophene Sulfone-Conjugated Microporous and Linear Polymers, *Chem. Mater.*, 2019, **31**, 305–313, DOI: **10.1021/acs.chemmater.8b02833**.

58 M. G. Mohamed, S. U. Sharma, N. Y. Liu, T. H. Mansoure, M. M. Samy, S. V. Chaganti, Y. L. Chang, J. T. Lee and S. W. Kuo, Ultrastable Covalent Triazine Organic Framework Based on Anthracene Moiety as Platform for High-Performance Carbon Dioxide Adsorption and Supercapacitors, *Int. J. Mol. Sci.*, 2022, **23**, 3174, DOI: **10.3390/ijms23063174**.

59 M. G. Mohamed, W. C. Chang, S. V. Chaganti, S. U. Sharma, J. T. Lee and S. W. Kuo, Dispersion of ultrastable crown-ether-functionalized triphenylamine and pyrene-linked porous organic conjugated polymers with single-walled carbon nanotubes as high-performance electrodes for supercapacitors, *Polym. Chem.*, 2023, **14**, 4589, DOI: **10.1039/D3PY00708A**.

60 A. O. Mousa, M. G. Mohamed, C. H. Chuang and S. W. Kuo, Carbonized Aminal-Linked Porous Organic Polymers Containing Pyrene and Triazine Units for Gas Uptake and Energy Storage, *Polymers*, 2023, **15**, 1891, DOI: **10.3390/polym15081891**.

61 Y. J. Li, L. Xu, H. B. Liu and Y. L. Li, Graphdiyne and graphyne: from theoretical predictions to practical construction, *Chem. Soc. Rev.*, 2014, **43**, 2572–2586, DOI: **10.1039/c3cs60388a**.

62 R. Matsuoka, R. Toyoda, R. Shiotsuki, N. Fukui, K. Wada, H. Maeda, R. Sakamoto, S. Sasaki, H. Masunaga, K. Nagashio, H. Nishihara, R. Matsuoka, R. Toyoda,

R. Shiotsuki, N. Fukui, K. Wada, H. Maeda and R. Sa, Expansion of the graphdiyne family: a triphenylene-cored analogue, *ACS Appl. Mater. Interfaces*, 2019, **11**, 2730–2733, DOI: **10.1021/acsami.8b00743**.

63 Z. Yao, Z. Zhang, J. Li, J. Jia, S. Ma, Y. Zhi, H. Xia and X. Liu, Fully π-conjugated, diyne-linked covalent organic frameworks formed via alkyne-alkyne cross-coupling reaction, *Mater. Chem. Front.*, 2022, **6**, 466–472, DOI: **10.1039/D1QM01322J**.

64 J. X. Jiang, F. Su, H. Niu, C. D. Wood, N. L. Campbell, Y. Z. Khimyak and A. I. Cooper, Conjugated Microporous Poly(Phenylene Butadiynylene)s, *Chem. Commun.*, 2008, 486–488, DOI: **10.1039/B715563H**.

65 X. M. Liu, Y. W. Zhang, H. Li, A. Sigen, H. Xia and Y. Mu, Triarylboron-Based Fluorescent Conjugated Microporous Polymers, *RSC Adv.*, 2013, **3**, 21267–21270, DOI: **10.1039/c3ra42801j**.

66 S. Luo, Z. Zeng, G. Zeng, Z. Liu, R. Xiao, P. Xu, H. Wang, D. Huang, Y. Liu, B. Shao, Q. Liang, D. Wang, Q. He, L. Qin and Y. Fu, Recent advances in conjugated microporous polymers for photocatalysis: designs, applications, and prospects, *J. Mater. Chem. A*, 2020, **8**, 6434–6470, DOI: **10.1039/D0TA01102A**.

67 Y. Song, P. C. Lan, K. Martin and S. Ma, Rational design of bifunctional conjugated microporous polymers, *Nanoscale Adv.*, 2021, **3**, 4891–4906, DOI: **10.1039/D1NA00479D**.

68 M. G. Mohamed, M. H. Elsayed, C. J. Li, A. E. Hassan, I. M. A. Mekhemer, A. F. Musa, M. K. Hussien, L. C. Chen, K. H. Chen, H. H. Chou and S. W. Kuo, Reticular design and alkyne bridge engineering in donor–π–acceptor type conjugated microporous polymers for boosting photocatalytic hydrogen evolution, *J. Mater. Chem. A*, 2024, **12**, 7693–7710, DOI: **10.1039/D3TA07309B**.

69 A. O. Mousa, Z. I. Lin, S. V. Chaganti, C. H. Chuang, C. K. Chen, S. W. Kuo and M. G. Mohamed, Bifunctional imidazolium linked tetraphenylethene based conjugated microporous polymers for dynamic antibacterial properties and supercapacitor electrodes, *Polym. Chem.*, 2024, **15**, 397–411, DOI: **10.1039/D3PY01303K**.

70 A. I. Said, M. G. Mohamed, M. Madhu, P. N. Singh, S. V. Chaganti, M. H. Elsayed, W. L. Tseng, F. M. Raymo and S. W. Kuo, Bifunctional luminescent conjugated microporous polymers containing BODIPY and tetraphenylethene units for highly efficient energy storage and enhanced sensing of Cu^{2+} ions, *Polymer*, 2024, **300**, 126988, DOI: **10.1016/j.polymer.2024.126988**.

71 S. Y. Chang, A. M. Elewa, M. G. Mohamed, I. M. A. Mekhemer, M. M. Samy, K. Zhang, H. H. Chou and S. W. Kuo, Rational design and synthesis of bifunctional Dibenzo[*g,p*]chrysene-based conjugated microporous polymers for energy storage and visible light-driven photo-

catalytic hydrogen evolution, *Mater. Today Chem.*, 2023, **33**, 101680, DOI: **10.1016/j.mtchem.2023.101680**.

72 S. Mushtaq, F. Meng, Z. Zhang, S. Bi and F. Zhang, Semiconducting three-dimensional polymeric frameworks with full sp/sp²-carbon skeletons for efficient photocatalysis, *Polym. Chem.*, 2023, **14**, 925–933, DOI: **10.1039/D2PY01439D**.

73 M. G. Mohamed, S. V. Chaganti, S. U. Sharma, M. M. Samy, M. Ejaz, J. T. Lee, K. Zhang and S. W. Kuo, Constructing Conjugated Microporous Polymers Containing the Pyrene-4,5,9,10-Tetraone Unit for Energy Storage, *ACS Appl. Energy Mater.*, 2022, **5**, 10130–10140, DOI: **10.1021/acsaem.2c01842**.

74 W. Lyu, C. Yan, Z. Chen, J. Chen, H. Zuo, L. Teng, H. Liu, L. Wang and Y. Liao, Spirobifluorene-Based Conjugated Microporous Polymer-Grafted Carbon Nanotubes for Efficient Supercapacitive Energy Storage, *ACS Appl. Energy Mater.*, 2022, **5**, 3706–3714, DOI: **10.1021/acsaem.2c00151**.

75 M. G. Mohamed, M. M. Samy, T. H. Mansoure, S. U. Sharma, M. S. Tsai, J. H. Chen, J. T. Lee and S. W. Kuo, Dispersions of 1,3,4-Oxadiazole-Linked Conjugated Microporous Polymers with Carbon Nanotubes as a High-Performance Electrode for Supercapacitors, *ACS Appl. Energy Mater.*, 2022, **5**, 3677–3688, DOI: **10.1021/acsaem.2c00100**.

76 A. O. Mousa, S. U. Sharma, S. V. Chaganti, T. H. Mansoure, P. N. Singh, M. Ejaz, C. H. Chuang, J. T. Lee, S. W. Kuo and M. G. Mohamed, Designing strategically functionalized conjugated microporous polymers with pyrene and perylenetetracarboxylic dianhydride moieties with single-walled carbon nanotubes to enhance supercapacitive energy storage efficiency, *J. Power Sources*, 2024, **608**, 234624, DOI: **10.1016/j.jpowsour.2024.234624**.

77 M. G. Mohamed, M. H. Elsayed, A. E. Hassan, A. Basit, I. M. A. Mekhemer, H. H. Chou, K. H. Chen and S. W. Kuo, Hybrid Porous Polymers Combination of Octavinylsilsesquioxane/Pyrene with Benzothiadiazole Units for Robust Energy Storage and Efficient Photocatalytic Hydrogen Production from Water, *ACS Appl. Polym. Mater.*, 2024, **6**, 5945–5956, DOI: **10.1021/acsapm.4c00655**.

78 N. T. Toan, D. Mohapatra, D. R. Kumar, M. Baynosa, S. Sahoo and J. Lee, Direct Growth of Nickel Cobalt Layered Double Hydroxide on Nickel Foam via Redox Reaction between Nitrate Ion and Ethanol for Hybrid Supercapacitors, *Electrochim. Acta*, 2021, **367**, 137226, DOI: **10.1016/j.electacta.2020.137226**.

79 K. V. Sankar and R. K. Selvan, The Ternary $MnFe_2O_4$/graphene/polyaniline Hybrid Composite as Negative Electrode for Supercapacitors, *J. Power Sources*, 2015, **275**, 399–407, DOI: **10.1016/j.jpowsour.2014.10.183**.